Supporting Information

An unusual 32-membered copper(II) metallomacrocube based on Cu_4O_3X cubic core: photocatalytic, electrocatalytic, and magnetic properties

Sisi Feng[a,b] · Fei Jia[a] · Liping Lu[a]* · Zhongping Li[c] · Shuo Zhang[a]

[a]Institute of Molecular Science, Key Laboratory of Chemical Biology and Molecular Engineering, Education Ministry, Shanxi University, Taiyuan, Shanxi 030006, P. R. China. E-mail: luliping@sxu.edu.cn, Fax: +86-351-7011022; Tel: +86-351-7017974

[b]State Key Laboratory of Coordination Chemistry, Nanjing University, Nanjing 210093, P. R. China

[c]Research Center of Environmental Science and Engineering, Shanxi University, Taiyuan 030006, P. R. China

1. Materials and Methods

All reagents and solvents were of standard commercial grade and directly used without further purification. Infrared (IR) spectra were obtained on a BRUKEP TENSOR27 spectrometer with KBr disks. Samples for elemental analysis experiments were dried under vacuum, and the analyses were performed with a CHN-O-Rapid instrument. Powder X-ray diffraction (PXRD) data were collected on a Bruker D8 Advance X-ray diffractometer with Cu $K\alpha$ radiation (λ = 1.5418Å). The simulated powder patterns were calculated by using Mercury 2.0 from the single crystal data. Variable temperature susceptibility measurements data were obtained with SQUID magnetometer (Quantum MPMS) in the temperature range of 2.0-300 K by using an applied field of 1000 *Oe*. The UV/visible spectra were recorded with a JASCO V-570 spectrophotometer. All electrochemical studies were conducted on an Electrochemical Workstation CHI 660B (CH Instruments, Austin, TX, USA). A 15-mL of electrolytic cell, an Ag/AgCl (saturated KCl)

reference electrode, a platinum foil auxiliary electrode, and a modified GC working electrode were used for electrochemical measurements. Thermogravimetric analysis was performed on a Labsys NETZSCH TG 209 Setaram apparatus with a heating rate of 10 ºC/min under a nitrogen atmosphere. The UV-Vis diffuse reflectance spectra (DRS) were recorded by a TU-1950 spectrophotometer, and the wavelength ranges from 200-800 nm. Liquid chromatography-mass spectrometry (LC–MS) was performed using Thermo Scientific Q Exactive.

2. Single Crystal X-ray Diffraction Analyses

Single-crystal X-ray diffraction data for complex **1** were collected in Beijing Synchrotron Radiation Facility (BSRF) beam line 3W1A which mounted with a MARCCD-165 detector (λ = 0.72000 Å) with storage ring working at 2.5 GeV. In the process, the crystals were protected by liquid nitrogen at 100(2) K. Data were collected by the program MARCCD and processed using HKL 2000[1].

The structure was solved by direct methods employed in the programs SHELXS-97[2] and refined by full-matrix least squares methods against F^2 with SHELXL-97[2]. Atoms of a benzene ring(C23, C24, C25, C26, C27, C28), DMF(C36, C37, C38, N11, O5, and water (O5A) were found to be disordered and were modelled over two sets of positions using restraints on their anisotropic displacement parameters. The major and minor disorder components had refined occupancies of 51 (1) and 49 (1)% for the benzene ring, 75 (1)% for the DMF and 25 (1)% for the water, respectively. A total of 213 restraints were used to refine the structural model owing to many atoms to be disordered. All the non-H atoms were refined anisotropically. Hydrogen atoms attached to C atoms were placed geometrically and refined using a riding model approximation, with C−H = 0.93−0.96 Å. Hydrogen atoms attached water and hydroxys were located from difference Fourier maps and refined using their global U_{iso} value with O−H = 0.82 Å. For complex **1** the *PLATON/SQUEEZE*[3] program was used to remove the contributions of all disordered water, DMFs and hydroxys solvent molecules or anion. The full details of the solvent removed are included in the platon squeeze details sections of the CIF. There is a total potential solvent accessible void 7699.1 Å^3 with 29.6% of per unit cell volume. Attempts to refine peaks of residual electron density as solvent molecules were unsuccessful. The residual electron density had a maximum 1.046 eÅ^{-3} out of [Cu_{32}] cluster. EA and TGA (Figure S10) results matched with the formula $C_{232.5}H_{275.5}Cl_8Cu_{32}N_{67.5}O_{57}$, corresponding to

$[(Cu_4Cl(OH)_3)_8(BI)_{24}(HBI)_6(H_2O)_{13.5}(DMF)_{4.5}]^{8+}\cdot 8OH^-\cdot 4H_2O\cdot 3DMF$.

A summary of the crystallographic data and data collection and refinement parameters for compound **1** is provided in Table S2. Crystallographic data in CIF format were deposited with the Cambridge Crystallographic Data Center as CCDC 1440536 for **1**. Selected bond lengths and angles for **1** are provided in Table S3.

3. Photocatalytic activity study

3.1 Photocatalytic decomposition experiments

The photocatalytic activities of the samples were evaluated by the degradation of RhB in the aqueous solution. 2.5 mL RhB aqueous solution with a concentration of 1.2×10^{-5} M was mixed with 1.4 mg of catalyst, and pretreatment of potocatalytic reaction was kept in dark before irradiation to reach the adsorption/desorption equilibrium, then it was exposed to illumination. Then, the samples were regularly taken out from the reactor and immediately centrifuged for the separation of any suspended solid. The transparent solution was transferred to trace cuvette and analyzed by a UV-vis spectrometer. A 300 W medium pressure mercury lamp served as an ultraviolet light source[4].

3.2 UV-Vis diffuse reflectance spectra (DRS)

UV-Vis DRS measured for powder of complex **1** is shown in Figure S6. The band gap energy (E_g) was determined from a plot of $(Ah\upsilon)^2$ versus photon energy ($h\upsilon$), where h – Planck constant, υ – frequency of electromagnetic wave, A – absorbancy.

3.3 Liquid chromatography-mass spectrometry (LC–MS)

To identify any reactive intermediates, 0.5 mL sample solution was taken before and after photocatalysis experiment, centrifuged in BD Falcon tubes at 7000 rpm and analyzed using Thermo Scientific Q Exactive. Separation of RhB and its decomposition products were done using a gradient elution in water and methyl alcohol mixtures of 70:30 for the first 5 min, 75:25 for the following 5 min, using a flow rate 0.2 mL min^{-1}. 5 μL was injected to the reverse phase column (Thermo Scientific Hypersil Jold C18 column 100 mm × 2.1 mm, 1.9 μm) using the autosampler at room temperature. The separated products were ionized using positive Electrospray Ionization (+ESI) technique.

4. Synthesis Procedures

4.1 Preparation of $[(Cu_4Cl(OH)_3)_8(BI)_{24}(HBI)_6(H_2O)_{13.5}(DMF)_{4.5}]^{8+}\cdot 8OH^-\cdot 4H_2O\cdot 3DMF$ (1)

A mixture of $CuCl_2\cdot 2H_2O$ (0.341 g, 2 mmol), TDB (1,2-di(1H-benzoimidazol-2-yl)ethane-1,2-diol)[5] (0.588 g, 2 mmol) and distilled water (18 ml, 1mol) in a molar ratio of 1:1:500 was mixed in a 25 ml stainless-steel reactor with a Teflon liner and heated from room temperature (RT) to 448 K in 0.5 h. The temperature was kept constant at 448 K for 92 h, then cooled down naturally to RT. The turbid solution was filtered off, and the precipitate was redissolved in DMF. The resulting mixture was stirred at ambient temperature for 30 min and then filtered. After several days, green cubic crystals of $[(Cu_4Cl(OH)_3)_8(BI)_{24}(HBI)_6(H_2O)_{13.5}(DMF)_{4.5}]^{8+}\cdot 8OH^-\cdot 4H_2O\cdot 3DMF$ (**1**) were isolated in 14% yield from the filtrate. Elemental Analysis for **1** ($C_{232.5}H_{275.5}Cl_8Cu_{32}N_{67.5}O_{57}$), calcd (%) C 38.55, H 3.83, N 13.05; found (%) C 38.40, H 3.49 N 13.21. IR (υ/cm^{-1}, s for strong, m medium, w weak): 3429m, 1649s, 1452s, 1388m, 1323m, 1279m, 1094s, 1038m, 862w, 748s, 665w, 619w, 493w.

4.2 Powder X-ray diffraction (PXRD)

PXRD pattern of **1** was determined at room temperature, and was found to match well with that simulated from its X-ray single crystal diffraction data, which confirmed the high purity of complex **1** (Figure S5b).

4.3 Thermogravimetric analyses (TGA) and Differential Scanning Calorimetry (DSC)

TGA and DSC curves of **1** were shown in Figure S10, which was consistent with the formula.

5. The bond valence sum (BVS) calculations

BVS calculations[6] are used to determine the oxidation states of Cu centers and the location of O/OH/H_2O groups (Table S4). Except for the BVS values 0.240, 0.278 of O4 and O7, respectively, indicating the state of the water molecules, the BVS values of others O atoms in complex **1** range from 1.065 – 1.181, indicating that these O atoms are monoprotonated. The +2 oxidation states of the Cu centers are also consistent with their coordination geometries (octahedron and tetragonal pyramid).

6. Supporting Scheme, Figures and Tables

Table S1. Cooper coordination discrete clusters with nuclearities higher than 30. (From CCDC database, up to November 2015)

Table S2. Crystal Data and Structure Refinement Parameters for Compound **1**

Table S3. Selected bond lengths(Å) and bond angles (°) of compound **1**

Table S4. BVS calculations of Cu centers and O in complex **1**

Figure S1. Asymmetric unit of complex **1**. Coordinated water molecules with lower occupancies, counter ions and solvent molecules were omitted for clarity.

Figure S2. View of the maximum diameter of 32-nuclear metallomacrocube unit of complex **1**. Coordinated water molecules with lower occupancies, H atoms, counter ions and solvent molecules were omitted for clarity.

Figure S3. Perspective view of the coordination modes of the Cu(II) ions for **1**.

Figure S4. Coordination orientations (a) and modes (b) of ligands in **1**.

Figure S5. a) The IR spectrum of RhB and complex **1** before and after the photocatalytic reaction; b) The PXRD of simulation of complex **1** and **1** before and after the photocatalytic reaction.

Figure S6. UV-Vis DRS K-M functions vs. energy (eV) of complex **1**.

Figure S7. LC–MS time resolved chromatogram and MS obtained before and after photocatalytic degradation of RhB.

Figure S8. Plots of I_p against $\upsilon^{1/2}$.

Figure S9. Temperature dependence of χ_m, $\chi_m T$, and χ_m^{-1} (inset) collected in applied field of 1000 Oe for complex **1**. Red solid line represents best fits.

Figure S10. TGA and DSC curves of **1**.

Scheme S1. Types of magnetic pathways in complex **1**.

Table S1. Cooper coordination discrete clusters with nuclearities higher than 30. (From CCDC database, up to November 2015)

Compound	Space group	References
$[Cu_{38}Se_4(SePh)_{24}(OAc)_6(PPh_2C_6H_4SMe)_4]\cdot 0.5dme$	Monoclinic, $P2_1/c$	*J.Chem.Soc.,Dalton Trans.,2002,* 4091-4094
$[PPN^+][Cl^-\subset\{[Cu(\mu\text{-}OH)(\mu\text{-}pz)]_{6+12}\}_2]\cdot[PPN^+]_2[SO_4^{2-}\subset\{Cu(\mu\text{-}OH)(\mu\text{-}pz)\}_{8+14+9}]$	Triclinic, *P*-1	*Angew.Chem.,Int.Ed.Engl.,2004,*43, 574-577
$[Cu_{44}Te_{23}(PPh_3)_{15}]$	Trigonal, *R*-3*c*	*Z.Anorg.Allg.Chem.,2000,*626,338-348

$[Cu_{44}Te_{23}(P^nPr_2Ph)_{15}]$	Hexagonal, *P*-6	*Z.Anorg.Allg.Chem.,2000,*626,338-348
$[Cu_{32}Se_7(Se\mathit{n}Bu)_{18}(P\mathit{i}Pr_3)_6]$	Monoclinic, $P2_1/n$	J. Chem. Soc., Dalton Trans., 1999, 1067-1076
$[Cu_{50}Se_{20}(Se\mathit{t}Bu)_{10}(P\mathit{i}Pr_3)_{10}]\cdot 2Et_2O$	Monoclinic, *C*2/*m*	J. Chem. Soc., Dalton Trans., 1999, 1067-1076
$[Cu_{38}Se_{13}(SePh)_{12}(dppb)_6]\cdot 4PhCH_3$	Triclinic, *P*-1	*Z.Anorg.Allg.Chem.,1999,*625**,**593-601
$[Cu_{36}Se_5(SePh)_{26}(dppa)_4]\cdot 2THF$	Monoclinic, *C*2/*c*	*Z.Anorg.Allg.Chem.,1999,*625,593-601
$[Cu_{32}Se_{16}(PPh_3)_{12}]\cdot 4THF$	Triclinic, *P*-1	*J.Chem.Soc.,DaltonTrans.,1998,* 2969-2972
$[Cu_{52}Se_{26}(PPh_3)_{16}]\cdot 2.5THF$	Triclinic, *P*-1	*J.Chem.Soc.,DaltonTrans.,1998,* 2969-2972
$[Cu_{30}Se_{15}(P\mathit{i}Pr_3)_{12}]$	Triclinic, *P*-1	*Angew.Chem.,Int.Ed.Engl.,1990,*29,796-799
$[Cu_{36}Se_{18}(P\mathit{t}Bu_3)_{12}]\cdot 6THF$	Monoclinic, *C*2/*c*	*Angew.Chem.,Int.Ed.Engl.,1990,*29,796-799
$[Cu_{50}S_{25}(P\mathit{t}Bu_2\ Me)_{16}]\cdot 1.5Et_2O$	Triclinic, *P*-1	*Chemistry-A European Journal,1996,2,* 1407-1416
$[Cu_{31}Se_{15}(SeSiMe_3)(P\mathit{t}Bu_2Me)_{12}]\cdot 0.5Et_2O$	Triclinic, *P*-1	*Chemistry-A European Journal,1996,2,* 1407-1416
$[Cu_{44}(\mu_8\text{-}Br)_2(\mu_3\text{-}OH)_{36}\text{-}(\mu\text{-}OH)_4(ntp)_{12}Br_8(OH_2)_{28}]Br_2\cdot 81H_2O$	Monoclinic, *C*2/*c*	*Inorg.Chem.,2004,*43,7269-7217
$\{[Cu_{12}(\mu_3\text{-}OMe)_2(\mu\text{-}OMe)_6(cpida)_6]^{2-}\{Cu_2(OMe)_2(MeOH)_3(NO_3)\}_2\cdot[Cu_{12}(\mu_3\text{-}OMe)_2(\mu\text{-}OMe)_6(cpida)_6]^{2-}[Cu_2(OMe)_2(MeOH)_2]\}_n\cdot 30nMeOH$	Triclinic, *P*-1	*Chem.Commun.,2002,*1054-1055
$[Cu_{39}\text{-}(TePh)_{11}Te_{16}(PEt_3)_{13}]$	Triclinic, *P*-1	*Inorg.Chem.,2001,*40,4678-4685
$[Cu_{32}As_{10}(dppm)_8]\cdot 5DME$	Monoclinic, $P2_1$/c	*Angew.Chem.,Int.Ed.Engl.,2000,*39, 3929-3933
$[Cu_{70}Se_{35}(PEt_2Ph)_{24}]$	Hexagonal, $P6_3$	*Isr.J.Chem.,2001,*41,31-38
$[Cu_{40}Se_{12}(Se_2fc)_8(PPh_3)_9]\cdot 2THF$	monoclinic, $P2_1/n$	*Organometallics,2005,*24,788-790
$As_4@[\{Cp^*Fe(\eta^5\text{-}P_5)\}_{10}Cu_{30}I_{30}(MeCN)_6]\cdot 2MeCN$	monoclinic, $P2_1/n$	*Angew.Chem.,Int.Ed.Engl.,2013,*52, 10896-10899
$P_4@[\{Cp^*Fe(\eta^5\text{-}P_5)\}_{10}Cu_{30}I_{30}(MeCN)_6]\cdot 2MeCN$	monoclinic, $P2_1/n$	*Angew.Chem.,Int.Ed.Engl.,2013,*52, 10896-10899
$[Cu_{40}Se_{16}(S\text{-}C_6H_4\text{-}CN)_8(dppm)_8]\cdot 6THF$	monoclinic, $P2_1/n$	*Z.Naturforsch.,Teil B,2013,*68,575-580
$(Bu_4N)_2[SO4^{2-}\subset\{cis\text{-}Cu^{II}(\mu\text{-}OH)(\mu\text{-}pz)\}_{8+14+9}]\cdot 2.5PhCH_3\cdot 2.5C_6H_{14}\cdot 0.5C_6H_{12}$	Triclinic, *P*-1	*Chem.Commun.,2012,*48,6860-6862
$(Bu_4N)_2[SO4^{2-}\subset\{cis\text{-}Cu^{II}(\mu\text{-}OH)(\mu\text{-}pz)\}_{8+14+9}]$	Triclinic, *P*-1	*Chem.Commun.,2012,*48,6860-6862
$(K^+\subset 18\text{-crown-}6)_2[SO4^{2-}\subset\{cis\text{-}Cu^{II}(\mu\text{-}$	Monoclinic, *C*2/*c*	*Chem.Commun.,2012,*48,6860-6862

OH)(μ-pz)}$_{8+14+9}$]		
[$Cu_{30}I_{16}$(mtpmt)$_{12}$(μ$_{10}$-S_4)]·3MeCN	Monoclinic, *C*2/*c*	*Chem.Commun.,2013,*49,4259-4261
[$Cu_{93}Se_{42}$(Se-C_6H_4-SMe)$_9$(PPh_3)$_{18}$]·3THF·15Et_2O	Triclinic, *P*-1	*Angew.Chem.,Int.Ed.Engl.,2010,*49, 6899-6903
[$Cu_{96}Se_{45}$(Se-C_6H_4-SMe)$_6$(PPh_3)$_{18}$]·21THF	Trigonal, *R*-3c	*Angew.Chem.,Int.Ed.Engl.,2010,*49, 6899-6903
[$Cu_{136}S_{56}$(S-CH_2-C_4H_3O)$_{24}$(dpppt)$_{10}$]·24$PhCH_3$	Monoclinic, *C*2/*c*	*Angew.Chem.,Int.Ed.Engl.,2010,*49, 6899-6903
[$Cu_{30}Fe_2Se_6$(SePh)$_{24}$(dppm)$_4$]·9THF	Monoclinic, *P*2$_1$/c	*Inorg.Chem.,2009,*48,8977-8984
[$Cu^I_{16}Cu^I_4$(μ$_6$-O)(OH)$_{18}$][Cu_6(μ3-OH)$_3$(enMe)$_3$(H_2O)$_3$(B-α-PW_9O_{34})]$_4$ ·4H_3O·2H_2O	Cubic, *P*-43n	*Inorg.Chem.,2009,*48,8294-8303
[Cu^I_{36}(Cu^IICl)$_2Se_{13}$(SePh)$_{12}$(dppe)$_6$] ·3EtOH	Trigonal, *R*-3	*Z.Naturforsch.,Teil B,2008,*63,941-944
[$Cu_{50}Se_{24}$(S-thiaz)$_2$(dppm)$_{10}$]·5DME	Monoclinic, *C*2/*c*	*Z.Anorg.Allg.Chem.2007,,*633,700-704
[$Cu_{48}Se_{24}$(S-thiazH)$_2$(dppm)$_{10}$]·4DME	Trigonal, *P*4$_2$/*n*	*Z.Anorg.Allg.Chem.2007,,*633,700-704
[$Cu_{84}Se_{42-x}S_x$(PEt_2Ph)$_{24}$](x ≈15)	Trigonal, *P*-3	*Z.Anorg.Allg.Chem.,2007,*633,2135-2137
Cu_{36}(fcSe_2)$_6Se_{12}$(P*n*Pr_3)$_{10}$($Ph_2P(CH_2)_3SH$)$_2$	monoclinic, *P*2$_1$/*n*	*Inorg.Chem.,2006,*45,9394-9401
$Cu_{36}Se_{12}$(fcSe_2)$_6$(P*n*Pr_2Ph)$_{12}$	monoclinic, *P*2$_1$/*n*	*Inorg.Chem.,2006,*45,9394-9401
[$Cu_{36}Se_8$(SPh)$_{20}$(PPh_3)$_8$]·DME	monoclinic, *P*2$_1$/*n*	*Eur.J.Inorg.Chem.,2005,*2306-2314
[$Cu_{54}Se_8$(SPh)$_{30}$(OAc)$_8$(PPh_3)$_6$]	Trigonal, *R*-3	*Eur.J.Inorg.Chem.,2005,*2306-2314
[$Cu_{40}Sb_{12}$(PMe_3)$_{20}$]·8THF	monoclinic, *P*2$_1$/*n*	*Angew.Chem.,Int.Ed.Engl.,2005,*44, 3932-3936
[$Cu_{32}S_5$(StBu)$_{16}$(hfa)$_6$]·CD_2Cl_2	Triclinic, *P*-1	*Angew.Chem.,Int.Ed.Engl.,2006,*45, 1733-1736
[Cu_{32}(H)$_{20}$\{S_2P(O*i*Pr)$_2$\}$_{12}$] ·4$CHCl_3$	Triclinic, *P*-1	Chem. Eur. J. 2015, 21, 1-7

Table S2. Crystal Data and Structure Refinement Parameters for Compound **1**

Compound	**1**
CCDC	1440536
Formula	$C_{232.5}H_{275.5}Cl_8Cu_{32}N_{67.5}O_{57}$
Fw	7244.69
Temp (K)	100(2)
Wavelength(Å)	0.72000
Crystal system	trigonal
Space group	*R*-3
a(Å)	23.108(3)
b (Å)	23.108(3)
c(Å)	56.327(11)

Vol (Å^3)	26048(8)
Z	3
D_c (g/cm^3)	1.386
μ(mm^{-1})	2.041
F(000)	10996
R_1 [I>2σ(I)],wR_2(all data)	0.0780, 0.2585
GOF on F^2	0.996
$\rho_{max,\ min}$,e(eÅ^{-3})	1.046/-0.880

$R_1 = \sum \frac{\|F_o| - |F_c\|}{|F_o|}$, $wR_2 = \sqrt{\frac{\sum w(F_o^2 - F_c^2)^2}{\sum w(F_o^2)^2}}$

Table S3. Selected bond lengths (Å) and bond angles (°) of compound **1.**

Cu(1)-O(1)	1.960 (5)	Cu(1)-N(3)	1.968 (6)
Cu(1)-N(1)	1.965 (6)	Cu(1)-O(2)	1.997 (5)
Cu(1)-Cl(1)	2.678 (2)	Cu(2)-N(5)	1.962 (7)
Cu(2)-O(1)	1.986 (5)	Cu(2)-O(3)	1.993 (5)
Cu(2)-N(4)^{i}	1.982 (7)	Cu(2)-Cl(1)	2.693 (2)
Cu(3)-N(7)	1.960 (7)	Cu(3)-N(2)^{ii}	1.966 (6)
Cu(3)-O(2)	1.984 (5)	Cu(3)-O(3)	1.986 (5)
Cu(3)-Cl(1)	2.660 (2)	Cu(4)-N(9)	1.960 (6)
Cu(4)-O(2)	2.020 (5)	Cu(4)-O(3)	2.098 (5)
Cu(4)-O(4)	2.183 (4)	Cu(4)-O(1)	2.220 (6)
Cu(4)-O(5)	2.355 (10)	Cu(4)-O(5A)	2.203 (13)
Cu(5)-N(6)	1.951 (7)	Cu(5)-N(8)^{iii}	1.974 (8)
Cu(5)-O(6)^{iii}	1.983 (6)	Cu(5)-O(6)	1.992 (6)
Cu(5)-Cl(2)	2.670 (2)	Cu(6)-O(6)	2.091 (6)
Cu(6)-O(6)^{iii}	2.091 (6)	Cu(6)-O(6)^{iv}	2.091 (6)
Cu(6)-O(7)^{iv}	2.128 (13)	Cu(6)-O(7)^{iii}	2.128 (13)
Cu(6)-O(7)	2.128 (13)	Cl(2)-Cu(5)^{iv}	2.670 (2)
Cl(2)-Cu(5)^{iii}	2.670 (2)	O(6)-Cu(5)^{iv}	1.982 (6)
N(2)-Cu(3)^{i}	1.966 (6)	N(4)-Cu(2)^{ii}	1.982 (7)
N(8)-Cu(5)^{iv}	1.974 (8)	Cu(3)-Cl(1)-Cu(1)	75.36 (6)
Cu(3)-Cl(1)-Cu(2)	74.57 (5)	Cu(1)-Cl(1)-Cu(2)	74.48 (6)
Cu(5)^{iv}-Cl(2)-Cu(5)	74.66 (8)	Cu(5)^{iv}-Cl(2)-Cu(5)^{iii}	74.66 (8)
Cu(5)-Cl(2)-Cu(5)^{iii}	74.66 (8)	Cu(1)-O(1)-Cu(2)	110.9 (3)
Cu(1)-O(1)-Cu(4)	96.6 (2)	Cu(2)-O(1)-Cu(4)	98.0 (2)
Cu(3)-O(2)-Cu(1)	110.1 (2)	Cu(3)-O(2)-Cu(4)	101.5 (2)
Cu(1)-O(2)-Cu(4)	102.1 (2)	Cu(2)-O(3)-Cu(3)	109.2 (2)
Cu(2)-O(3)-Cu(4)	101.9 (2)	Cu(3)-O(3)-Cu(4)	98.8 (2)
Cu(5)^{iv}-O(6)-Cu(5)	109.1 (3)	Cu(5)^{iv}-O(6)-Cu(6)	100.0 (3)
Cu(5)-O(6)-Cu(6)	99.7 (3)		

Symmetry codes: (i) *y, -x+y, -z*; (ii) *x-y, x, -z*; (iii) *-x+y, -x, z*; (iv) *-y, x-y, z*.

Table S4. BVS calculations of Cu centers and O in complex **1**

Bond type	Bond distance (Å)	Bond valence		Sum of Bond valance	
		Cu(I)	Cu(II)	Cu(I)	Cu(II)
Cu(1)-O(1)	1.960 (5)	0.346	0.439	1.450	2.004
Cu(1)-O(2)	1.997 (5)	0.313	0.397		
Cu(1)-N(1)	1.965 (6)	0.345	0.506		
Cu(1)-N(3)	1.968 (6)	0.342	0.502		
Cu(1)-Cl(1)	2.678 (2)	0.104	0.160		
Cu(2)-O(1)	1.986 (5)	0.322	0.409	1.415	1.956
Cu(2)-O(3)	1.993 (5)	0.316	0.401		

Cu(2)-N(4)^{i}	1.982 (7)	0.329	0.483		
Cu(2)-N(5)	1.962 (7)	0.348	0.510		
Cu(2)-Cl(1)	2.693 (2)	0.100	0.153		
Cu(3)-O(2)	1.984 (5)	0.324	0.411		
Cu(3)-O(3)	1.986 (5)	0.322	0.409	1.448	2.006
Cu(3)-N(2)^{ii}	1.966 (6)	0.344	0.505		
Cu(3)-N(7)	1.960 (7)	0.349	0.513		
Cu(3)-Cl(1)	2.660 (2)	0.109	0.168		
Cu(4)-O(1)	2.220 (6)	0.171	0.217		
Cu(4)-O(2)	2.020 (5)	0.294	0.373		
Cu(4)-O(3)	2.098 (5)	0.238	0.302	1.405	1.853
Cu(4)-O(4)	2.183 (4)	0.189	0.240		
Cu(4)-O(5)	2.355 (10) 25%	0.119	0.151		
Cu(4)-O(5A)	2.203 (13) 75%	0.179	0.227		
Cu(4)-N(9)	1.960 (6)	0.349	0.513		
Cu(5)-O(6)	1.992 (6)	0.317	0.402		
Cu(5)-O(6)^{iii}	1.983 (6)	0.325	0.412	1.442	1.997
Cu(5)-N(6)	1.951 (7)	0.358	0.526		
Cu(5)-N(8)^{iii}	1.974 (8)	0.336	0.494		
Cu(5)-Cl(2)	2.670 (2)	0.106	0.163		
Cu(6)-O(6)	2.091 (6)	0.243	0.308		
Cu(6)-O(6)^{iii}	2.091 (6)	0.243	0.308		
Cu(6)-O(6)^{iv}	2.091 (6)	0.243	0.308	1.389	1.758
Cu(6)-O(7)	2.128 (13)	0.220	0.278		
Cu(6)-O(7) ^{iii}	2.128 (13)	0.220	0.278		
Cu(6)-O(7) ^{iv}	2.128 (13)	0.220	0.278		
O atoms					
Cu(1)-O(1)	1.960 (5)		0.439		
Cu(2)-O(1)	1.986 (5)		0.409		1.065
Cu(4)-O(1)	2.220 (6)		0.217		
Cu(1)-O(2)	1.997 (5)		0.397		
Cu(3)-O(2)	1.984 (5)		0.411		1.181
Cu(4)-O(2)	2.020 (5)		0.373		
Cu(2)-O(3)	1.993 (5)		0.401		
Cu(3)-O(3)	1.986 (5)		0.409		1.112
Cu(4)-O(3)	2.098 (5)		0.302		
Cu(4)-O(4)	2.183 (4)		0.240		0.240
Cu(5)-O(6)	1.992 (6)		0.402		
O(6)-Cu(5) ^{iv}	1.982 (6)		0.413		1.123
Cu(6)-O(6)	2.091 (6)		0.308		
Cu(6)-O(7)	2.128 (13)		0.278		0.278

Symmetry codes: (i)*y,-x+y,-z*;(ii)*x-y,x,-z*;(iii)*-x+y,-x,z*;(iv) *-y,x-y,z*.

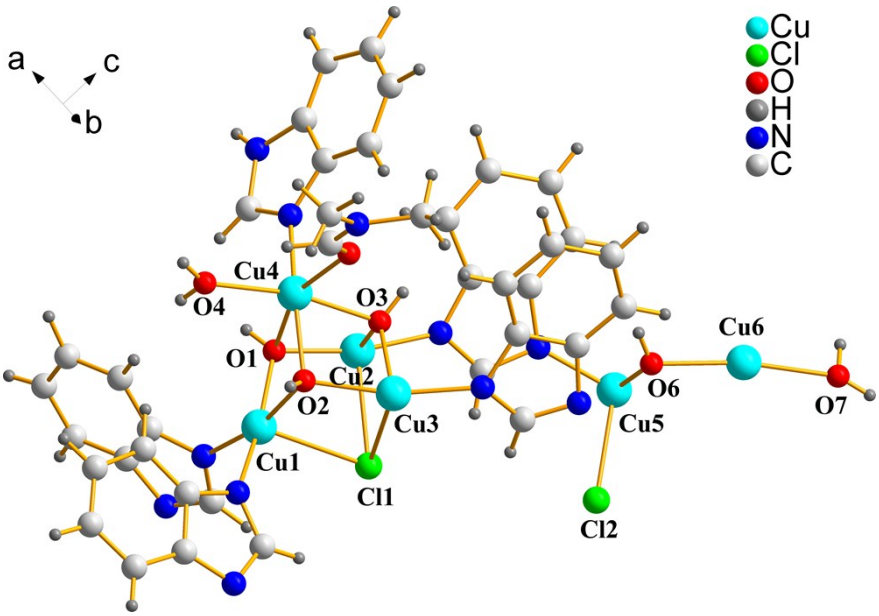

Figure S1. Asymmetric unit of complex **1**. Coordinated water molecules with lower occupancies, counter ions and solvent molecules were omitted for clarity.

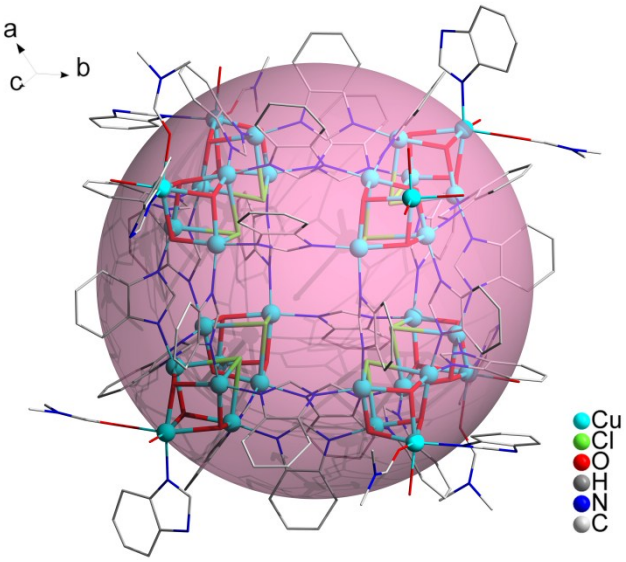

Figure S2. View of the maximum diameter ~18 Å of the vertices of the big cube (pink ball) of complex **1**. Coordinated water molecules with lower occupancies, H atoms, counter ions and solvent molecules were omitted for clarity.

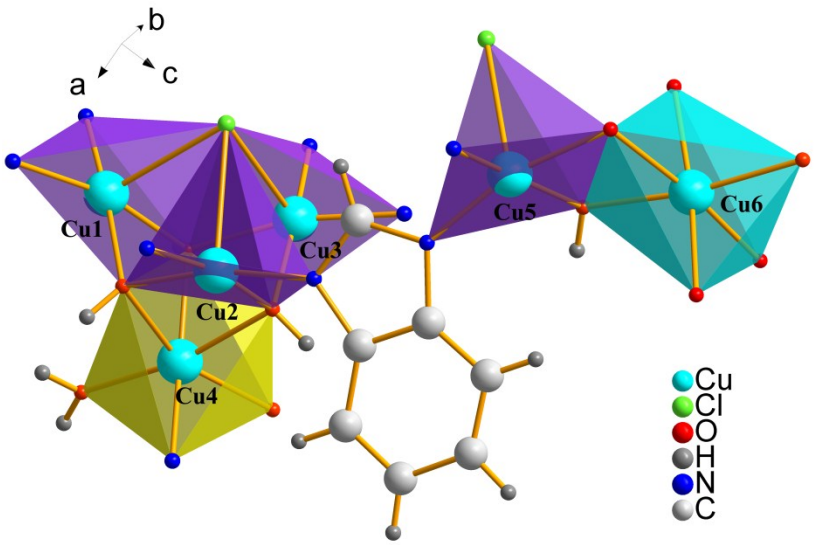

Figure S3. Perspective view of the coordination modes of the Cu(II) ions for **1**.

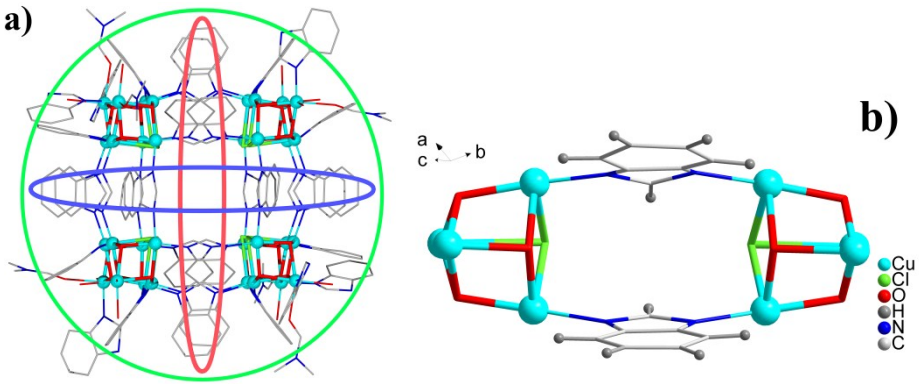

Figure S4. Coordination orientations (a) and modes (b) of the ligands in **1**.

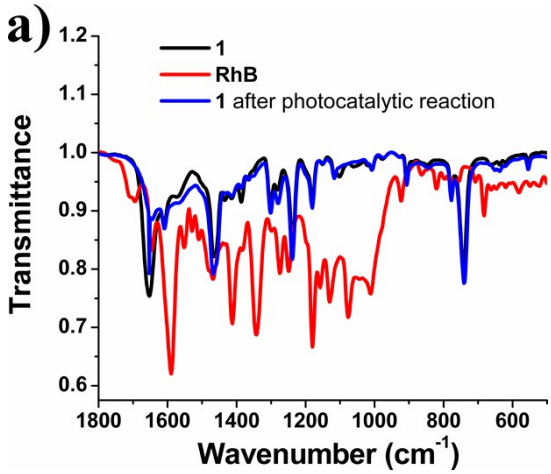

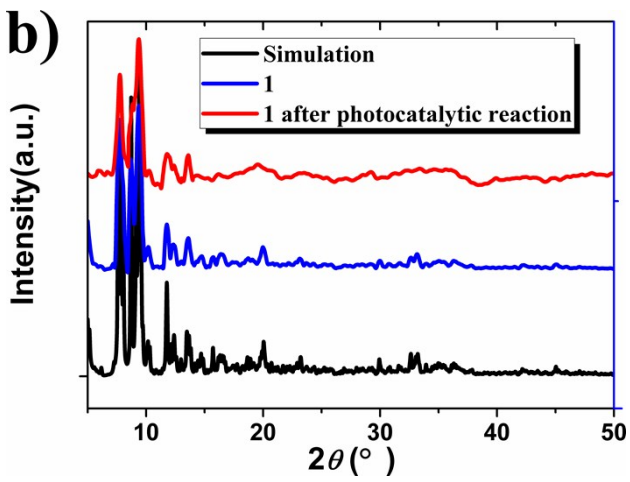

Figure S5. a) The IR spectrum of RhB and complex **1** before and after the photocatalytic reaction; b) The PXRD of simulation of complex **1** and **1** before and after the photocatalytic reaction.

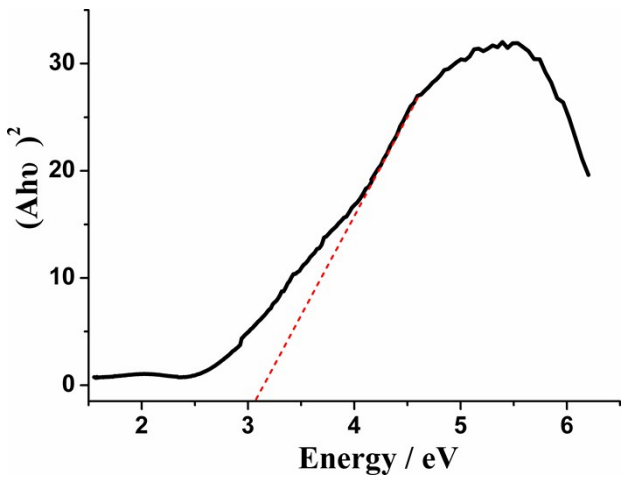

FigureS6. UV-Vis DRS K-M functions vs. energy (eV) of complex **1**.

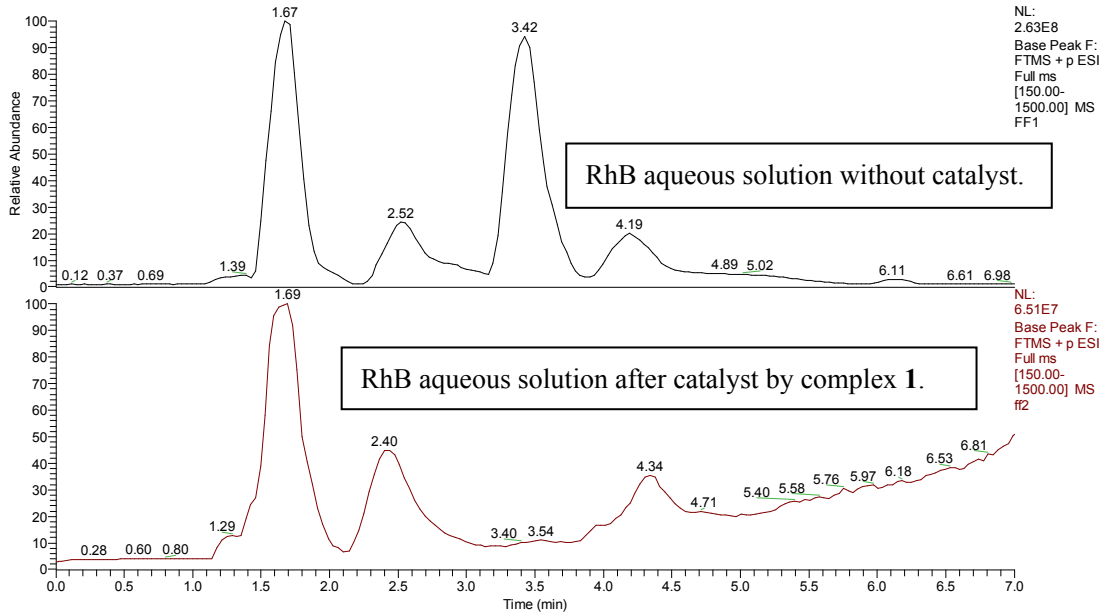

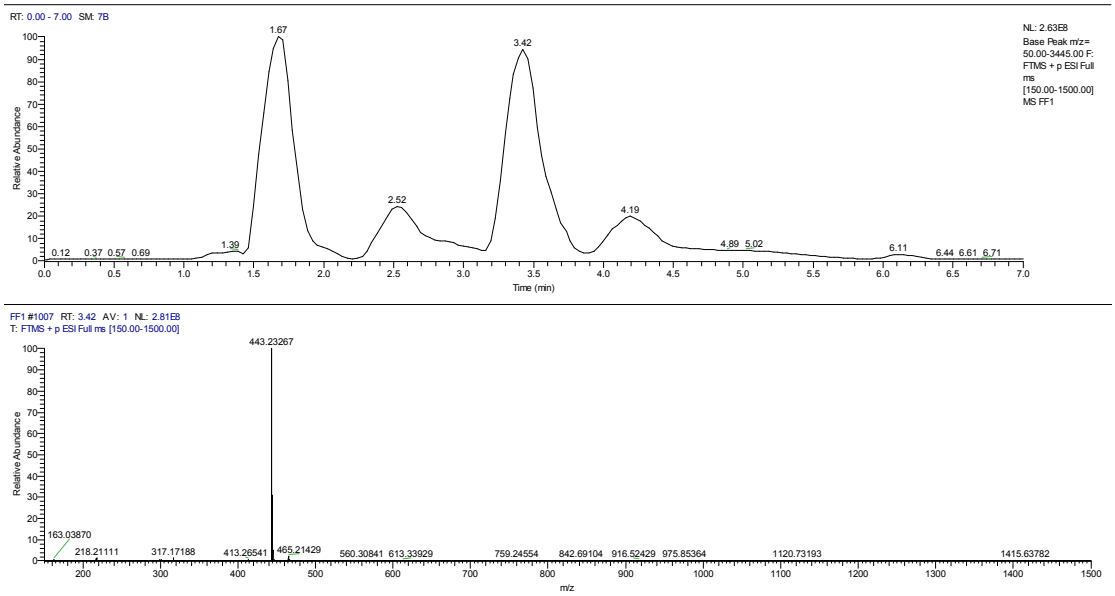

FigureS7. LC–MS time resolved chromatogram and MS obtained before and after photocatalytic degradation of RhB.

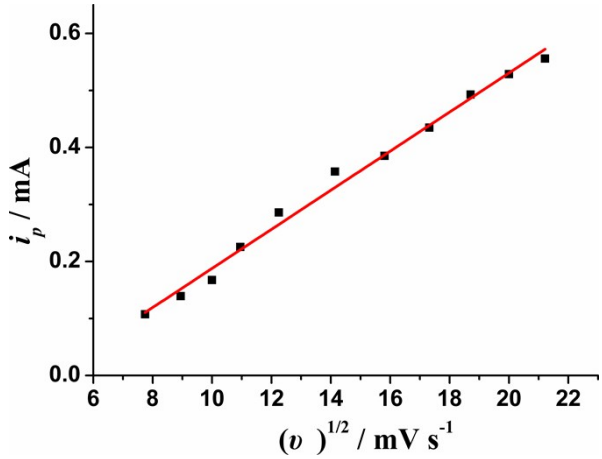

Figure S8. Plots of I_p against $\upsilon^{1/2}$.

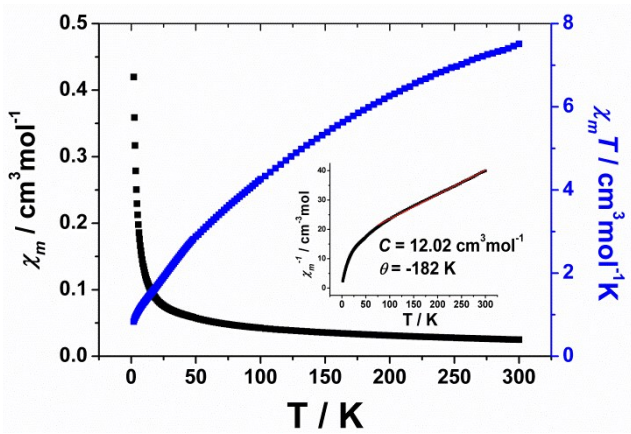

Figure S9. Temperature dependence of χ_m ,$\chi_m T$, andχ_m^{-1}(inset) collected inapplied field of 1000 Oe for complex **1**. Red solid line represents best fits.

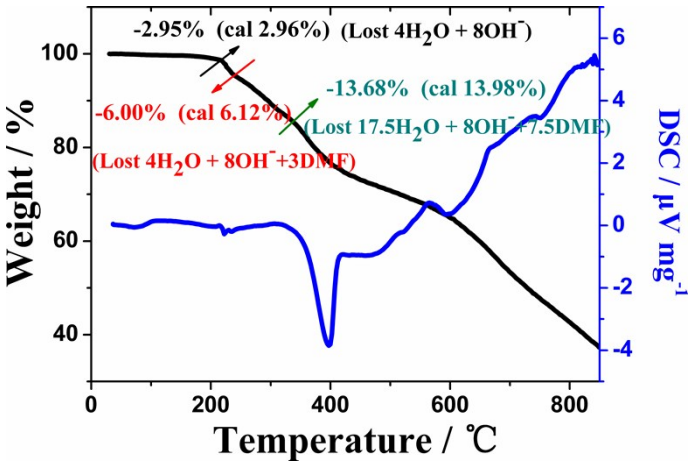

FigureS10. TGA and DSC curves of **1**.

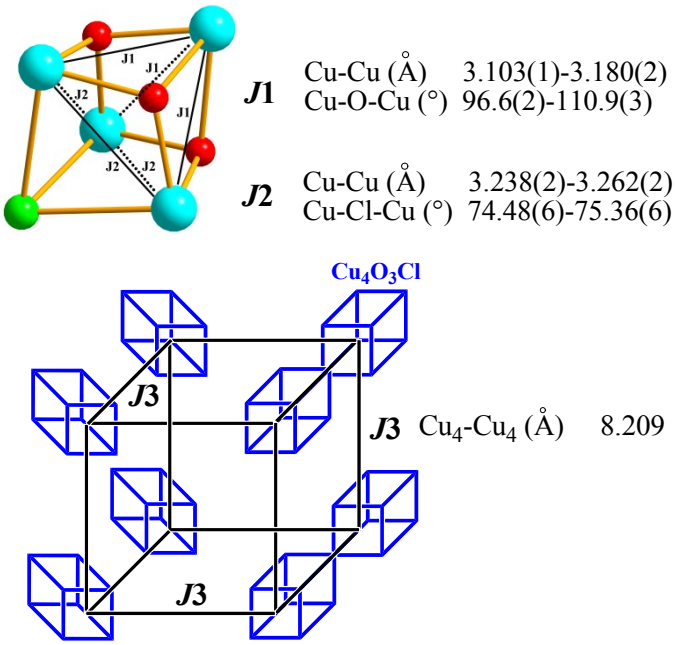

Scheme S1. Types of magnetic pathways in complex **1**.

7. Reference

1. Z. Otwinowski and W.Minor, *Methods Enzymol.* 1997, **276**, 307-326.
2. G. M. Sheldrick, *Acta Crystallogr.* 2008, **A64**, 112-122.
3. A. L. Spek, *Acta Cryst.* 2009, **D65**, 148-155.
4. X. Xu, X. Gao, T. Lu, X. Liu and X. Wang, *J. Mater. Chem. A*, 2015, **3**, 198-206.
5. (a) S. S. Feng, M. L. Zhu, L. P. Lu, L. Du, Y. B. Zhang and T. W. Wang, *Dalton Trans.*, 2009, 6385-6395; (b) S. S. Feng, M. L. Zhu, L. P. Lu and M. L. Guo, *Chem. Commun.*, 2007, 4785-4787.
6. I. D. Brown, *Chem. Rev.*, 2009, **109**, 6858-6919.